

EXPERIMENTAL BENCHMARKING OF WAKEFIELDS AT THE FERMI FEL LINAC AND UNDULATOR LINE

S. Di Mitri^{†,1,2}, L. Sturari¹, Elettra Sincrotrone Trieste, Trieste, Italy
C. Venier, R. Vescovo, University of Trieste, Dept. of Engineering, Trieste, Italy
²also at University of Trieste, Dept. of Physics, Trieste, Italy

Abstract

Collective effects such as wakefields affect the dynamics of high brightness electron beams in linear accelerators (linacs), and can degrade the performance of short wavelength free-electron lasers (FELs). If a reliable model of wakefields is made available, the accelerator can be designed and configured with parameters that minimize their disrupting effect. In this work, the simulated effect of geometric (diffractive) wakefields and of coherent synchrotron radiation on the electron beam energy distribution at the FERMI FEL is benchmarked with measurements, so quantifying the accuracy of the model. Wakefields modelling is then extended to the undulator line, where particle tracking confirms the limited impact of the resistive wall wakefield on the lasing process. The study reveals an overall good understanding of collective effects in the facility.

INTRODUCTION

At the FERMI FEL [1,2], a systematic study of collective effects has been carried out since the early stage of machine design [3–7]. In the last decade, numerical predictions were benchmarked with experimental results to demonstrate the interplay of longitudinal geometric wakefields and beam current profile [8,9], to quantify the effect of transverse wakefields on the beam projected emittance [10,11], and to compare 1- vs. 3-dimensional CSR effects on the beam emittance [12–14]. They all confirm, on top of the routine operation of the facility, that the electron beam dynamics is strongly affected by geometric (diffractive) wakefields in the linac sections (L0–L4 in Fig.1), and by CSR emission in the magnetic chicane devoted to bunch length compression (BC1). In addition to this, a semi-analytical formulation of the resistive wall wakefield in the undulator elliptical vacuum chamber was provided [15]. Still, a systematic characterization of the longitudinal wakefields acting in the linac, as well as a start-to-end particle tracking run in the presence of resistive wall wakefield in the undulator line, is lacking. The present work targets these two points.

After a theoretical introduction to wakefields, we complement the aforementioned studies by investigating the effect of linac geometric wakefields and of CSR on the beam energy distribution. The effect is quantified by measuring the beam mean energy and energy spread in a spectrometer line installed at the linac end, as function of bunch length and bunch charge. The final bunch length is determined by magnetic compression, and it was varied by scanning the RF phase of the upstream linac. The bunch charge was varied by changing the intensity of the laser pulse that drives

the photoelectron emission at the Gun cathode. The study is extended to the computation and simulation of resistive wall wakefields in the FERMI FEL-2 undulator vacuum chamber. This is the second and longer undulator line of the two currently installed at FERMI. It is devoted to the emission of the shortest FEL wavelengths, in the range 4–20 nm, and it is expected to be more sensitive to the degradation of electron beam brightness.

The FERMI layout is sketched in Fig.1. The electron beam is generated in the RF Gun by photoelectron emission from a Copper cathode illuminated by a UV laser. Electrons are accelerated up to 1.5 GeV in the L0–L4 S-band linac sections. It is time-compressed, nominally by a factor ~ 10 , in the BC1 bunch compressor, at the energy of 0.3 GeV (BC2 is not used routinely). Each linac section includes different travelling wave accelerating structures, which are grouped by length and inner geometry. They are of type “INJ” (3.2 m-long each; 9 mm average radius), “LIL” (4.5 m-long each; 10 mm average radius), “BTW” (6.1 m-long each; 5 mm average radius), and “X-band” (0.75 m-long; 5 mm average radius). “LH” stays for laser heater. The whole linac is 175 m long. The Spreader transfer line is ~ 30 m long. The FEL-1 and FEL-2 undulator lines are, respectively, 30 m and 44 m long.

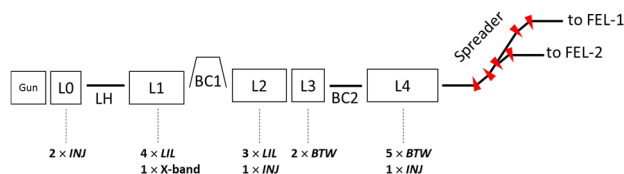


Figure 1: Sketch (not to scale) of the FERMI electron beam delivery system. Published in [16].

WAKEFIELDS MODEL

Geometric Wakefield in RF Cavities

The analytical expressions of the FERMI linac wake functions, in unit of V/(pC m), are given in Eq.1, and are plotted in Fig.2. They well represent the e.m. field pattern established along the whole multi-cell accelerating structure, and apply to bunch lengths shorter than 5 mm [3,5]. The upper-case label of each wake function refers to the structures naming in Fig.1. Please note that the numerical coefficients are consistent with the s-coordinate expressed in units of meter.

$$w_i^{INJ}(s) = 380 \cdot e^{-\sqrt{\frac{s}{1.28 \cdot 10^{-3}}}}$$

$$w_i^{LIL}(s) = 311 \cdot e^{-\sqrt{\frac{s}{1.38 \cdot 10^{-3}}}} \quad (1)$$

[†] simone.dimitri@elettra.eu

$$w_i^{BTW}(s) = 1226 \cdot e^{-\sqrt{\frac{s}{3 \cdot 10^{-4}}}} + \frac{0.494}{\sqrt{s}} + 494 \cdot \sqrt{s}$$

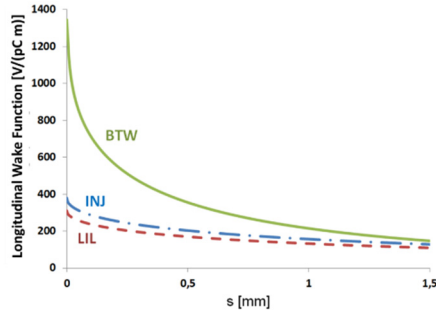


Figure 2: Geometric longitudinal wake functions per unit length associated to the diverse inner geometries of the FERMI S-band accelerating structures, see Eq.1. Labels refer to the structures naming adopted in Fig.1. Published in [16].

Resistive Wall Wakefield in Undulator Chamber

The FERMI undulator vacuum chamber is made of 1.1 m-long sections in Stainless Steel 304LN, of cylindrical cross section and 11 mm inner radius. These are interleaved by 3.2 m-long elliptical chambers in Aluminum, of inner diameters 7 mm × 22 mm. Since the ellipticity of the elliptical chambers is larger than 3, the wake function can be approximated to that of parallel plates at a gap equal to the shortest (vertical) diameter [15].

The longitudinal resistive wall impedance of a cylindrical metallic vacuum chamber of inner radius b and conductivity σ_{AC} is [17]:

$$Z_{AC}^{cyl}(k) = \frac{Z_0}{2\pi b} \left(\frac{f(k)}{k} - i \frac{kb}{2} \right)^{-1} \quad (2)$$

The wake function is calculated as the inverse-Fourier transform of Eq.2:

$$G_{L,AC}(z) = \frac{2c}{\pi} \int_0^\infty \text{Re}[Z_{AC}(k)] \cos(kz) dk \quad (3)$$

The analytical expression of the longitudinal resistive wall impedance of parallel plates is known from the Bane and Stupakov model in the limit $s_1 \ll b$, where $s_1 = \sqrt[3]{\frac{2b^2}{Z_0\sigma_{DC}}}$ estimates the distance at which the wakefield associated to σ_{AC} in a cylindrical pipe of inner radius b is damped [18,19]. That condition is satisfied at FERMI, and the wake function is calculated as the inverse-Fourier transform of the following impedance:

$$Z_{AC}^{pp}(k) = \frac{Z_0}{4\pi} \int_{-\infty}^{+\infty} \left(\frac{f(k)}{k} (\cosh(bx))^2 - i \frac{k}{x} \cosh(bx) \sinh(bx) \right)^{-1} dx \quad (4)$$

Coherent Synchrotron Radiation

In the FERMI BC1, most of the CSR physics is described by the steady-state emission [12,14], which is represented by the impedance per unit length [20]:

$$Z_{CSR}(k) = \frac{Z_0 k^{1/3}}{\pi R^{2/3}} (0.41 + i0.23) \quad (5)$$

The 1-D approximation is expected to fail for bunches approaching full compression, *i.e.*, upright longitudinal phase space. In this case, CSR direct transverse forces and the dependence of the longitudinal electric field on the transverse coordinates become important. Since the elegant code, used in the following, projects the charge distribution onto a line-charge, an artificially stronger CSR interaction is expected to be simulated, whereas the actual interaction is somehow “diluted” in the transverse plane [14].

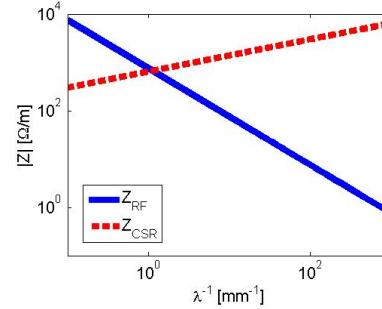


Figure 3: Spectral behaviour of the RF geometric (Eq.1) and CSR impedance (Eq.5) per unit length. Z_{RF} is calculated for an iris radius of 5 mm (average value in the FERMI BTW structures), Z_{CSR} is calculated for a curvature radius of 4 m (typical of FERMI BC1). Published in [16].

WAKEFIELDS BENCHMARKING

Linac

The effect of wakefields on the particle dynamics in FERMI was simulated with elegant. The code convolutes the charge distribution produced by tracking with geometric wake functions provided as external text files. CSR is simulated in the 1-D approximation, including entrance and exit transient effects. The quantities in Eq.2 predicted by the code at the linac end were compared with the corresponding measured quantities. Table 1 summarizes the main linac and electron beam parameters adopted in the experiment and used in the simulations.

Table 1: FERMI Electron Beam and Linac Parameters for the Nominal Bunch Length Compression Factor. Asterisk marks simulated-only parameters.

Parameter	Value	Units
Charge	0.35, 0.70	nC
Peak Current at Injector Exit	35*, 70*	A
Linac-1 RF Phase	116.5	deg
Energy at BC1	0.28	GeV
BC1 Dipole Bending Angle	85	mrad
BC1 Compression Factor	10*, 11	
Final Peak Current (bunch core)	400*, 750	A
Final Bunch Duration, fwhm	0.3*, 0.8	ps
Energy Spread at Linac End, rms	1.2, 1.9	MeV
Mean Energy at Linac End	1.45	GeV

The RF phase of L1 was varied in the code in order to scan the final bunch length. Finally, the mean energy and energy spread predicted by the code were compared with

measured quantities, as illustrated in Fig.4. The comparison was repeated at the bunch charge of 0.35 nC and 0.70 nC. In both cases the largest discrepancy between experiment and simulation is in correspondence of 117.5 deg RF phase, *i.e.*, at the point of full compression. Left plot suggests that the 1-D CSR modeling in `elegant` overestimates the strength of the interaction for full compression (compare red dashed line with solid blue line). In the right plot, the discrepancy at the phase of full compression is due to the discrepancy in the energy spread induced by CSR, which sums to that one determined by the RF curvature and longitudinal geometric wakefields. In other words, Instead, an excellent agreement is obtained both in mean energy and energy spread for all other RF phases. In addition to this, Fig.4 confirms that the longitudinal effect of CSR is negligible w.r.t. the linac geometric impedance for bunch lengths longer than $\sim 50 \mu\text{m}$.

The successful benchmarking of simulation and experiment results for RF phases far from the point of full compression confirms the reliability of the model adopted for the linac geometric wakefields. Moreover, one is allowed to infer that the linac geometric wakefields dominate the beam dynamics over other collective effects not considered here, such as space charge forces in the main linac, geometric wakefields associated to discontinuities of the beam pipe outside the accelerating structures, and linac resistive wall wakefield.

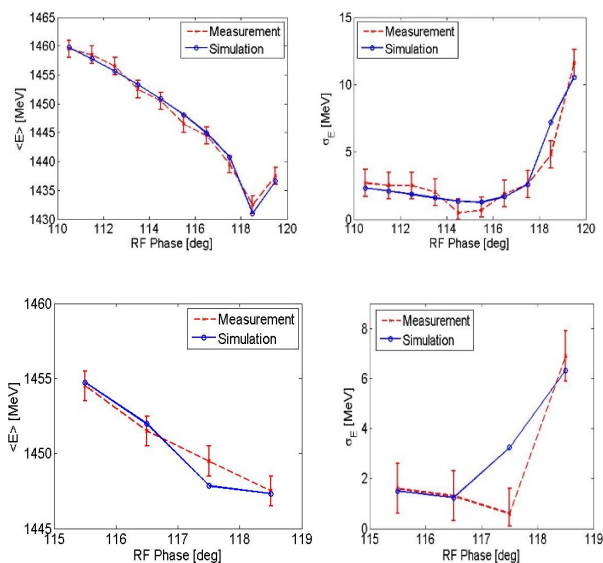


Figure 4: Simulated and measured beam mean energy (left) and rms energy spread (right) at the linac end as function of the L1 RF phase, for 0.7 nC (top) and 0.35 nC bunch charge (bottom). Each measured data is the average of 10 consecutive measurements. Published in [16].

Undulator

The FERMI FEL-2 undulator vacuum chamber is made of Aluminum elliptical sections, surrounded by undulators, alternated with Stainless Steel cylindrical sections, surrounded by other magnetic and diagnostic elements. The longitudinal resistive wall wake function was calculated as

the inverse-Fourier transform of Eq.2 for the cylindrical sections, and of Eq.4 for the elliptical sections. Figure 5 compares the simulated electron beam longitudinal phase space at the end of the undulator line, with and without resistive wall wakefields. Particle tracking reveals that only a ~ 100 fs-long portion of the bunch head is affected by resistive wall wakefields; even in that region, the energy spread is weakly affected, at the level of 0.1%. Owing to the fact that the VUV seed laser that initiates the FEL process at FERMI is typically ~ 70 fs long or shorter, that it is superimposed to the central portion of the bunch and with relative arrival time jitter smaller than 50 fs, we can reasonably conclude that the resistive wall wakefield is predicted to have no impact on the lasing efficiency.

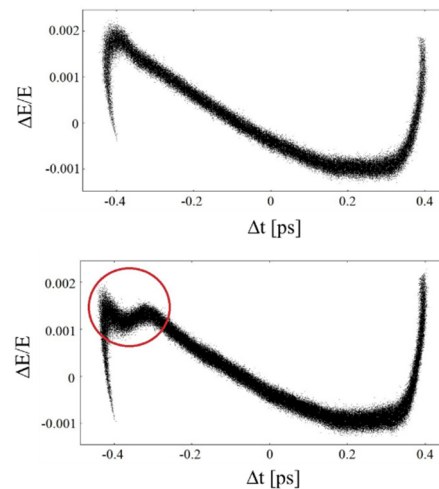


Figure 5: Simulated longitudinal phase space at the end of the FERMI FEL-2 undulator line, without (top) and with (bottom) resistive wall wakefields. The red circle highlights the region of the bunch head in which wakefields have most effect. Published in [16].

CONCLUSIONS

The study confirms that the linac geometric wakefields dominate the longitudinal beam dynamics at the FERMI nominal working point, together with the RF curvature. CSR plays an important role only at rms bunch lengths shorter than $50 \mu\text{m}$, whereas nominal bunch durations at FERMI are longer than $70 \mu\text{m}$. Particle tracking through the undulator line in the presence of resistive wall wakefields confirms the limited impact of that impedance on the beam quality, thus on the lasing process.

REFERENCES

- [1] E. Allaria, R. Appio, L. Badano, W.A. Barletta, S. Basanese, S.G. Biedron, A. Borgia, E. Busetto, D. Castronovo, P. Cinquegrana, et al., “Highly coherent and stable pulses from the FERMI seeded free-electron laser in the extreme ultraviolet”, *Nature Photon.*, Vol. 6 (2012) 699–704. doi:10.1038/nphoton.2012.233
- [2] E. Allaria, D. Castronovo, P. Cinquegrana, P. Craievich, M. Dal Forno, M. Danailov, G. D’Auria, A. Demidovich, G. De Ninno, S. Di Mitri, et al., “Two-stage seeded soft-X-ray

- free-electron laser”, *Nature Photon.* Vol 7 (2013),913–918. doi:10.1038/nphoton.2013.277
- [3] P. Craievich, T. Weiland, and I. Zagorodnov, ”The short-range wakefields in the BTW accelerating structure of the ELETTRA LINAC”, *Nucl. Instr. Meth. Phys. Research A*, vol. 558 (2006), 58-61. doi:10.1016/j.nima.2005.11.069
- [4] P. Craievich, S. Di Mitri and A. A. Zholents, ”Single-bunch emittance preservation in the presence of trajectory jitter for FERMI@elettra-seeded FEL”, *Nucl. Instr. and Methods in Phys. Res. A*, vol. 604, (2009) 457–465. doi:10.1016/j.nima.2009.03.106
- [5] P. Craievich, *Short-range longitudinal and transverse wakefield effects in FERMI@Elettra FEL project*, Ph.D. thesis, Technische Universiteit Eindhoven, Department of Applied Physics, Eindhoven, The Netherlands, ISBN 978-90-386-2294-1 (2010).
- [6] S. Di Mitri et al., ”Design and simulation challenges for FERMI@elettra”, *Nucl. Instr. and Methods in Phys. Res. A*, vol. 608, (2009) 19–27. doi:10.1016/j.nima.2009.06.028
- [7] S. Di Mitri, ”Machine Design and Electron Beam Control of a Single-Pass Linac for Free Electron Laser: the FERMI@Elettra Case Study”, Ph.D. Thesis, *University of Gronigen, Zernike Institute for Advanced Materials*, ISBN 978-90-367-5176-6 (2011).
- [8] M. Cornacchia, S. Di Mitri, G. Penco and A. A. Zholents, ”Formation of electron bunches for harmonic cascade x-ray free electron lasers”, *Phys. Rev. Special Topics – Accel. and Beams*, vol. 9, 120701 (2006). doi:10.1103/PhysRevSTAB.9.120701
- [9] G. Penco, M. Danailov, A. Demidovich, E. Allaria, G. De Ninno, S. Di Mitri, W.M. Fawley, E. Ferrari, L. Giannessi, and M. Trovo’, ”Experimental Demonstration of Electron Longitudinal-Phase-Space Linearization by Shaping the Photoinjector Laser Pulse”, *Phys. Rev. Letters*, vol. 112, 044801 (2014). doi:10.1103/PhysRevLett.112.044801
- [10] S. Di Mitri, ”Maximum brightness of linac-driven electron beams in the presence of collective effects”, *Phys. Rev. Special Topics – Accel. and Beams*, vol. 16, 050701 (2013). doi:10.1103/PhysRevSTAB.16.050701
- [11] S. Di Mitri, L. Froehlich and E. Karantzoulis, ”Influence of longitudinally tapered collimators on a high brightness electron beam”, *Phys. Rev. Special Topics – Accel. and Beams*, vol. 15, 061001 (2012). doi:10.1103/PhysRevSTAB.15.061001
- [12] S. Di Mitri, E. M. Allaria, P. Craievich, W. Fwaley, L. Giannessi, A. Lutman, G. Penco, S. Spampinati and M. Trovo’, ”Transverse emittance preservation during bunch compression in the Fermi free electron laser”, *Phys. Rev. Special Topics – Accel. and Beams*, vol. 15, 020701 (2012). doi:10.1103/PhysRevSTAB.15.029901
- [13] S. Di Mitri, M. Cornacchia, and S. Spampinati, ”Cancellation of Coherent Synchrotron Radiation Kicks with Optics Balance”, *Phys. Rev. Letters*, vol. 110, 014801 (2013). doi:10.1103/PhysRevLett.110.014801
- [14] A. Brynes, et al., ”Beyond the limits of 1D coherent synchrotron radiation”, *New J. Phys.*, vol. 20, 073035 (2018). doi:10.1088/1367-2630/aad21d
- [15] A. Lutman, R. Vescovo, P. Craievich, ”Electromagnetic field and short-range wake function in a beam pipe of elliptical cross section”, *Phys. Rev. Special Topics – Accel. and Beams*, vol. 11, 074401 (2008). doi:10.1103/PhysRevSTAB.11.074401
- [16] S. Di Mitri, L. Sturari, C. Venier, Ro. Vescovo, ”Wakefield benchmarking at a single-pass high brightness electron linac”, *Phys. Rev. Accel. and Beams*, vol. 22, 014401 (2019). doi:10.1103/PhysRevAccelBeams.22.014401
- [17] B. W. Zotter, S. A. Kheifets, ”Impedances and Wakes in High-Energy Particle Accelerators”, *World Scientific Publishing Co. Pte. Ltd.*, Singapore (1998). doi:10.1142/3068
- [18] K. L. F. Bane and G. Stupakov, ”Resistive Wall Wakefield in the LCLS undulator”, in *Proc. PAC2005.*, Knoxville, Tennessee, USA (2005) 3391. doi:10.1109/PAC.2005.1591481
- [19] H. Henke and O. Napoly, ”Wake fields between two parallel resistive plates”, in *Proc. 2nd EPAC 90.*, Nice, France (1990),p. 1046-1048.
- [20] J. B. Murphy, S. Krinsky, and R. L. Gluckstern, ”Longitudinal Wakefield for Synchrotron Radiation”, in *Proc. PAC 95*, Dallas, TX, USA, (1995). doi:10.1109/PAC.1995.505757

Content from this work may be used under the terms of the CC BY 3.0 licence (© 2019). Any distribution of this work must maintain attribution to the author(s), title of the work, publisher, and DOI